A master equation approach to the dynamics of zero electron kinetic energy (ZEKE) states and ZEKE spectroscopy

Yi-Hsieh Wang, H. Mineo, S. D. Chao, H. L. Selzle, H. J. Neusser, E. W. Schlag, Y. Teranishi, and S. H. Lin

Citation: The Journal of Chemical Physics **134**, 064316 (2011); doi: 10.1063/1.3547363
View online: http://dx.doi.org/10.1063/1.3547363
View Table of Contents: http://scitation.aip.org/content/aip/journal/jcp/134/6?ver=pdfcov
Published by the AIP Publishing

A master equation approach to the dynamics of zero electron kinetic energy (ZEKE) states and ZEKE spectroscopy

Yi-Hsieh Wang,[1] H. Mineo,[2] S. D. Chao,[2,a)] H. L. Selzle,[3] H. J. Neusser,[3] E. W. Schlag,[3] Y. Teranishi,[4] and S. H. Lin[1,4,5]
[1]*Institute of Chemistry, Academia Sinica, Taipei 115, Taiwan*
[2]*Institute of Applied Mechanics, National Taiwan University, Taipei 106, Taiwan*
[3]*Institut für Physikalische und Theoretische Chemie, Technische Universität München, Lichtenbergstr. 4, D-85748 Garching, Germany*
[4]*Institute of Applied Chemistry, Institute of Molecular Science, Chiao-Tung University, Hsin-Chu, Taiwan*
[5]*Institute of Atomic and Molecular Sciences, Academia Sinica, Taipei 106, Taiwan*

(Received 19 August 2010; accepted 5 January 2011; published online 11 February 2011)

We have theoretically studied important dynamic processes involved in zero electron kinetic energy (ZEKE) spectroscopy using the density matrix method with the inverse Born–Oppenheimer approximation basis sets. In ZEKE spectroscopy, the ZEKE Rydberg states are populated by laser excitation (either a one- or two-photon process), which is followed by autoionizations and *l*-mixing due to a stray field. The discrimination field is then applied to ionize loosely bound electrons in the ZEKE states. This is followed by using the extraction field to extract electrons from the ZEKE levels which have a strength comparable to that of the extraction field. These extracted electrons are measured for the relative intensities of the ion states under investigation. The spectral positions are determined by the applied laser wavelength and modified by the extraction electric field. In this paper, all of these processes are conducted within the context of the density matrix method. The density matrix method can provide not only the dynamics of system's population and coherence (or phase) but also the rate constants of the processes involved in the ZEKE spectroscopy. Numerical examples are given to demonstrate the theoretical treatments. © *2011 American Institute of Physics*. [doi:10.1063/1.3547363]

I. INTRODUCTION

Zero electron kinetic energy (ZEKE) spectroscopy was first reported by Müller-Dethlefs and co-workers in 1984[1,2] as a high resolution photoelectron spectroscopy (PES) of parent neutrals. Moreover, new laser spectroscopy methods, such as mass analyzed threshold ionization spectroscopy,[3] threshold ion-pair production spectroscopy,[4] and the Rydberg-tagging time-of-flight method,[5] employ detection concepts similar to those used in the ZEKE spectroscopy. These techniques have been widely used in different circumstances including the detection of short-lived resonance states in chemical reactions.[6] This has raised considerable interest in understanding of the behavior of molecules with energies very close to their ionization thresholds.

The capability of the ZEKE technique to determine ionization potential (IP) of molecules and ionic rovibronic energies with high accuracy is widely recognized and has been illustrated in many systems. However, the interpretation of rotational-line intensities and dynamics of ZEKE states still poses some problems.[7–9] In a ZEKE experiment, the observed spectral intensities result from a series of dynamic processes. The laser pumping (preparation) of the high Rydberg states is followed by intricate channel couplings, autoionization, *l*-level mixing, and final field extraction (detection) processes. Obtaining a systematic and coherent understanding of these dynamic processes requires a methodology which can allow transparent calculations from first principles and easy interpretation. In a recent paper,[10] we demonstrated how to use the inverse Born–Oppenheimer approximation (IBOA) (Fig. 1) as a basis set to study the vibrational and rotational autoionizations using H_2 as an example. The present paper continues that study to determine the relationship between the ZEKE line intensities and ionization cross-sections and to examine whether zero electron kinetic energy photoelectron spectroscopy intensities are consistent with the conventional PES intensities, which can be predicted by the *ab initio* calculations. Rotational and vibrational autoionizations are believed to play important roles in the measurement of ZEKE spectra intensities. Anomalous intense peaks are often observed in ZEKE spectroscopy[7] and they are usually attributed to resonance effects. How should we approach these resonance phenomena? In this paper we approach these questions through ZEKE spectroscopy theory based on the use of the IBOA (Refs. 10–12) and the density matrix method. It should be noted that previous studies make frequent use of the multichannel quantum defect theory (MQDT),[8,13,14] which is combined with the photoelectron spectroscopy model.[15–20]

Since the measurements of ZEKE spectra consist of a series of processes, the density matrix method is an ideal technique because the master equations (MEs) can be derived for each process. These MEs can then be solved sequentially given proper experimental conditions such as frequencies,

a)Author to whom correspondence should be addressed. Electronic mail: sdchao@iam.ntu.edu.tw.

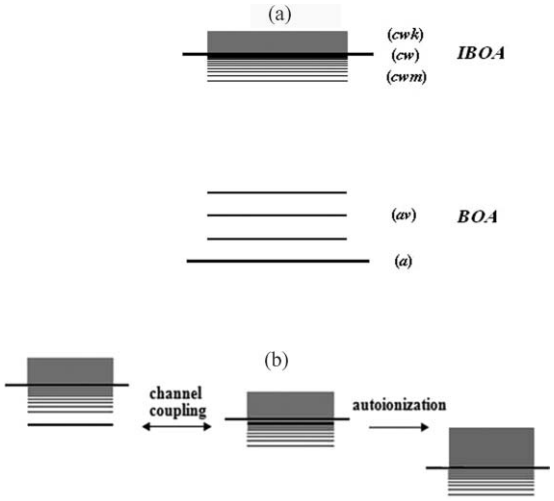

FIG. 1. (a) The Born–Oppenheimer approximation (BOA) and inverse Born–Oppenheimer approximation (IBOA). (b) Autoionization and channel coupling.

intensities, pulse duration of the pumping laser, and the time-durations of *l*-mixing, discrimination field, and extraction fields. Solving this series of MEs obtains the intensity of ZEKE electrons associated with the ZEKE spectra and provides insight into the most detailed dynamics associated with these states.

The present paper is organized as follows. Section II briefly describes the density matrix method and the IBOA, which are used to establish a proper basis sets for studying the ZEKE dynamics and spectroscopy. This is followed by theoretical treatments of rotational and vibrational autoionization processes (Sec. III) and the *l*-level mixing by a stray field (Sec. IV). In Sec. V, the optical absorption rate constants for one- and two-photon absorption for ZEKE spectroscopy are derived. The ionization of ZEKE levels induced by the discrimination and extraction fields is presented in Sec. VI.

II. GENERAL CONSIDERATION

The observed ZEKE band-shapes should depend on optical excitation (or pumping) of ZEKE levels, rotational and vibrational autoionizations,[9,21–23] *l*-mixing induced by a stray field,[24] electric field-induced lowering of ionization thresholds, and field-induced ionization due to the discrimination and extraction fields.[7] This paper uses the density matrix method to study the ZEKE spectroscopy by including these processes. It is well known that the density matrix method can describe not only individual processes but also the entire experiment taking all the individual processes into account. Furthermore, the density matrix can provide information on the dynamics of the population and coherence (or phase) of the systems as a function of time.[25,26]

The starting point of the density matrix method is the Liouville equation,

$$\frac{d\hat{\rho}}{dt} = -\frac{i}{\hbar}[\hat{H}, \hat{\rho}] - \hat{\Gamma}\hat{\rho}, \tag{2.1}$$

where $\hat{H}$ and $\hat{\rho}$, respectively, represent the molecular Hamiltonian and the density matrix of the molecule and $\hat{\Gamma}$ denotes the damping operator due to the interaction between the molecule and the radiation field. The diagonal matrix elements of $\hat{\rho}$ represent the population of the molecule, while the off-diagonal matrix elements of $\hat{\rho}$ denote molecule's coherence (or phase).

The interaction between the laser and molecule should be included in Eq. (2.1),

$$\frac{d\hat{\rho}}{dt} = -\frac{i}{\hbar}[\hat{H}, \hat{\rho}] - \frac{i}{\hbar}[\hat{V}(t), \hat{\rho}] - \hat{\Gamma}\hat{\rho}. \tag{2.2}$$

The dipole approximation is commonly used in $\hat{V}(t)$. We can apply Eqs. (2.1) and (2.2) to the ZEKE spectroscopy. The observed ZEKE signals start with optical excitation (or pumping) by one or two lasers. This step is described by Eq. (2.2); the laser frequency, intensity, pulse duration, etc., are involved in $\hat{V}(t)$. The detailed derivation and solution of Eq. (2.2) are given in Sec. V, providing information on population and coherence at the end of optical pumping. The evolution of the system is then described by Eq. (2.1). Given the autoionization of the ZEKE levels and the presence of a stray field, $\hat{H}$ should be written as $\hat{H} = \hat{H}_0 + \hat{H}' + \hat{H}''$, where $\hat{H}_0$ denotes the zero-order Hamiltonian of the molecule, while $\hat{H}'$ and $\hat{H}''$ describe the autoionization and *l*-mixing by a stray field (Sec. IV). Finally, the discrimination field and extraction field are applied to obtain the ZEKE signal; in this case, Eq. (2.1) can also be used, where $\hat{H} = \hat{H}_0 + \hat{H}''$, except that the electric field involved in $\hat{H}''$ is different from that for the stray field (see Sec. VI).

Having chosen the IBOA as a basis set for the theoretical treatments of ZEKE experiments,[10,11] here we briefly describe the IBOA [see Fig. 1(a)]. The molecular Hamiltonian in this case can be expressed as

$$\hat{H} = \hat{H}_{\text{ion}} + \hat{T}_e, \tag{2.3}$$

where $\hat{H}_{\text{ion}}$ is the Hamiltonian of the ion core and $\hat{T}_e$ denotes the kinetic energy operator of the ZEKE electron. $\hat{H}_{\text{ion}}$ is given by

$$\hat{H}_{\text{ion}} = -\frac{\hbar^2}{2m_e}\sum_{i=1}^{n-1}\nabla_i^2 + \hat{T}_N + V, \tag{2.4}$$

where i denotes the ith electron in the ion core and $\hat{T}_N$ denotes the kinetic energy operator of the nuclei. Since the ZEKE electron moves slowly and has low kinetic energy, we can first neglect $\hat{T}_e$ and derive the ionic Schrödinger equation

$$\hat{H}_{\text{ion}}\Theta_{cw} = U_{cw}\Theta_{cw}. \tag{2.5}$$

Using the expansion theorem, we can expand the total wavefuntion Ψ in terms of Θ_{cw}, $\Psi = \sum_{cw'}\Phi_{cw'}\Theta_{cw'}$.

Substituting Ψ into the full Schrödinger equation, we have

$$\sum_{cw'} \hat{T}_e \left(\Phi_{cw'}\Theta_{cw'}\right) + \sum_{cw'} U_{cw'} \left(\Phi_{cw'}\Theta_{cw'}\right) = E \sum_{cw'} \Phi_{cw'}\Theta_{cw'} \tag{2.6}$$

and

$$\begin{aligned}\hat{T}_e \left(\Phi_{cw'}\Theta_{cw'}\right) = {} & \Theta_{cw'}\hat{T}_e\Phi_{cw'} - \frac{\hbar^2}{2m_e} \\ & \times \left(2\nabla_e\Theta_{cw'}\cdot\nabla_e\Phi_{cw'} + \Phi_{cw'}\nabla_e^2\Theta_{cw'}\right) \\ = {} & \Theta_{cw'}\hat{T}_e\Phi_{cw'} + \hat{H}'_{\mathrm{IBO}}\left(\Phi_{cw'}\Theta_{cw'}\right), \end{aligned} \tag{2.7}$$

where "e" denotes the ZEKE electron. Since the ionic wavefunction varies indirectly with the ZEKE electron coordinate, we can neglect the terms involving $\hat{H}'_{\mathrm{IBO}}$ in Eq. (2.7). Multiplying Eq. (2.6) by and Θ_{cw}, integrating the ionic coordinates, we obtain

$$(\hat{T}_e + U_{cw})\Phi_{cwm} = E_{cwm}\Phi_{cwm}, \tag{2.8}$$

and the total wavefuntion is denoted by

$$\Psi_{cwm} = \Phi_{cwm}\Theta_{cw}. \tag{2.9}$$

This shows that the ZEKE electron is moving in the potential energy surface provided by the ion core described by (cw). Here, c and w, respectively, represent the electronic state and the rotation–vibration state of the ion core, and m denotes the quantum number of the ZEKE electron. The states below the rovibronic state (cw) of the ion are discrete (cwm), while those above (cw) are continuous(cwk). Here we refer to the high Rydberg states near but below the ionization continuum as "ZEKE Rydberg" states (or simply ZEKE states).

Applying the multipole expansion to the ZEKE electron-core Coulomb interaction and keeping only the monopole term, we can derive the unperturbed (zero-order) Hamiltonian and wavefunctions. Thus, Eqs. (2.5) and (2.8) can be expressed as

$$\hat{H}^0_{\mathrm{ion}}\Theta^0_{cw}(\vec{R}) = U^0_{cw}\Theta^0_{cw}(\vec{R}), \tag{2.10}$$

$$\left(\hat{T}_e - \frac{e^2}{r}\right)\Phi^0_m(\vec{r}) = E^0_m\Phi^0_m(\vec{r}), \tag{2.11}$$

where $\Phi^0_m(\vec{r})$ is the hydrogenic wavefunction characterized by the quantum numbers $m = (n,l,m)$ and Θ^0_{cw} represents the pure ionic wavefunction characterized by the vibration and rotation quantum numbers v^+ and N^+. It should be noted that c is assumed as the electronic ground state of the ion and is neglected in the following expressions. The total zero-order wavefunction is denoted by

$$\begin{aligned}\left|\Psi^0_{cwm}\right\rangle &= |nl\ v^+N^+J\ M_J\rangle \\ &= R_{nl}(r)\,\chi_{v^+}(R)\sum_{mM^+} C^{lN^+}_{mM^+;JM_J} \\ &\quad \times Y_{lm}(\theta,\phi)\,Y_{N^+M^+}(\Theta,\Phi). \end{aligned} \tag{2.12}$$

In Eq. (2.12), R_{nl} represents the radial wavefunction of the ZEKE electron; χ_{v^+} represents the vibrational wavefunction of the ion; Y_{lm} and $Y_{N^+M^+}$ are, respectively, the spherical harmonics of the electronic angular momentum l and the rotational angular momentum N^+. With the Clebsch–Gordan coefficient $C^{lN^+}_{mM^+;JM_J}$, we use the representation of the total angular momentum J, and its projection M_J. The higher multipole terms neglected in Eqs. (2.11) and (2.12) will be used to calculate the channel coupling effect in the following discussion.[10,27]

At the zero-order basis, the IBOA is the same as that in Hund's case (d) where the electronic orbital angular momentum and the rotational angular momentum are decoupled.[10] However, differences appear as one calculates transition probabilities. In the IBOA form, the terms neglected in Eq. (2.7) can be used as the perturbative interaction, which refers to the breakdown of IBOA, $\hat{H}'_{\mathrm{IBO}}$.[10,12] Similar to the radiationless transitions of excited electronic states, which are attributed to the breakdown of Born–Oppenheimer approximation (BOA) (e.g., internal conversion and intersystem crossing),[28] $\hat{H}'_{\mathrm{IBO}}$ is responsible for the radiationless transitions of the ZEKE states (e.g., autoionization).

Figure 1(b) schematically shows autoionization and channel coupling based on the IBOA. In our model, channel coupling (or "forced autoionization" in Ref. 7) is responsible for the intensity borrowing in the ZEKE spectra, while the autoionization, which is described in Sec. III, determines the lifetime of the ZEKE states.

Here, we discuss how to calculate the intensity borrowing in the rotationally resolved ZEKE spectrum of H_2 for $X\,^2\Sigma^+_g(v^+ = 2) \leftarrow X\,^1\Sigma^+_g(v^+ = 0)$.[21] In the following, the rotational transition is denoted by (N^+, J''), where N^+ and J'' represent the final and initial rotational quantum numbers in the above vibronic states. In the H_2 ZEKE spectrum, it was reported that some rotational-line intensities deviate from the simulated intensities.[21] As an example, consider the rotational transition (0, 2). As mentioned in Ref. 21, the experimental intensity for this transition is 51 [relative to 100 for (1, 1)], while the theoretical intensity is only 2.8. Merkt and Softley[21] attributed this intensity enhancement to the channel interaction between the ZEKE state of $N^+ = 0$ and the low n Rydberg state of $N^+ = 2$.[7,21] Softley and Hudson further incorporated the channel interaction and simulated the spectrum by using the MQDT, and their simulation results were in agreement with the experiment.[29] Here, we shall study this effect using the multipole interaction as the perturbation with the IBOA basis set.

For H_2, the matrix element of the quadrupole interaction can be written as[27,30]

$$\begin{aligned}&\langle n'l'\mathrm{v}^+N^{+\prime}J'\ M_J'|V'_{\mathrm{quad}}|nl\ v^+N^+J\ M_J\rangle \\ &= \langle\chi_{v+}|Q(R)|\chi_{v+}\rangle\langle R_{n'l'}|r^{-3}|R_{nl}\rangle \\ &\quad\times\left[\frac{4\pi}{5}\sum_{mM^+}\sum_{m'M'^+}\sum_{\bar{m}} C^{lN^+}_{mM^+;JM_J}C^{l'N^{+\prime}}_{m'M^{+\prime};J'M'_J}\right. \\ &\quad\left.\times\langle Y_{l'm'}|Y_{2\bar{m}}|Y_{lm}\rangle\left\langle Y_{N'^+M'^+}\left|Y^*_{2\bar{m}}\right|Y_{N^+M^+}\right\rangle\right] \\ &= \langle\chi_{v^+}|Q(R)|\chi_{v^+}\rangle\langle R_{n'l'}|r^{-3}|R_{nl}\rangle \\ &\quad\times g(l',N^{+\prime},J',M'_J;l,N^+,J,M_J), \end{aligned} \tag{2.13}$$

where $Q(R)$ denotes the quadrupole moment of the ion, whose numerical data for H_2^+ are given in Ref. 31 The

bound–bound hydrogenic radial integral can be evaluated analytically[10] and, using the 3-*j* and 6-*j* symbols, the angular matrix element g is given by[24,32]

$$g\left(l', N^{+\prime}, J', M'_J; l, N^+, J, M_J\right) = (-1)^{l+l'+J} \times \left\{ \begin{array}{ccc} J & N^{+\prime} & l' \\ 2 & l & N^+ \end{array} \right\} \delta_{J',J}\delta_{M'_J,M_J} \times \left[\left(2l'+1\right)(2l+1)\right]^{1/2} \left(\begin{array}{ccc} l' & 2 & l \\ 0 & 0 & 0 \end{array} \right) \times \left[\left(2N^{+\prime}+1\right)\left(2N^{+}+1\right)\right]^{1/2} \left(\begin{array}{ccc} N^{+\prime} & 2 & N^+ \\ 0 & 0 & 0 \end{array} \right). \tag{2.14}$$

By taking this coupling effect as the perturbation, the ZEKE state can be expressed as

$$\Psi_{n,N^+} = \left|\Psi^0_{n,N^+}\right\rangle + C_{n,N^+;n',N^{+\prime}} \left|\Psi^0_{n',N^{+\prime}}\right\rangle \tag{2.15}$$

and

$$C_{n',N^{+\prime};n,N^+} = \frac{\left\langle \Psi^0_{n',N^{+\prime}}\right| V'_{\text{quad}} \left|\Psi^0_{n,N^+}\right\rangle}{E^0_{n,N^+} - E^0_{n',N^{+\prime}}}. \tag{2.16}$$

For convenience, we use the quantum numbers (n, N^+) and (n', $N^{+\prime}$) to, respectively, denote the relevant ZEKE eigenstate and its coupling Rydberg eigenstate. The matrix element in Eq. (2.16) is the coupling matrix element in Eq. (2.13).

For example, we consider the rotational transition (0, 2) of H_2. In this case, we select $n = 100$ for the ZEKE state of $N^+ = 0$ (with respect to the reduced IP by the discrimination field $F = 3$ V/cm) and $n = 26$ for the Rydberg state of $N^+ = 2$. In addition, the corresponding orbital quantum numbers $l = l\prime = 1$. Thus, we obtain

$$\Psi_{100,0^+} = |100, 0^+\rangle + C_{26,2^+;100,0^+}|26, 2^+\rangle, \tag{2.17}$$

where

$$C_{26,2^+;100,0^+} = \frac{\langle 26, 2^+|V'_{\text{quad}}|100, 0^+\rangle}{E_{100,0^+} - E_{26,2^+}} = 0.052. \tag{2.18}$$

Thus, the transition dipole moment from ($J'' = 2$) can be expressed as

$$\langle \Psi_{100,0^+}|\mu|\Psi_{J''=2}\rangle = \langle 100, 0^+|\mu\,|\Psi_{J''=2}\rangle + C_{26,2^+;100,0^+}\langle 26, 2^+|\mu|\Psi_{J''=2}\rangle. \tag{2.19}$$

As reported by Xie and Zare,[16] the theoretical transition moment for the transition (0, 2) is small, while that for (2, 2) is large. Therefore, from Eq. (2.19), we can see that the (0, 2) transition borrows its intensity from (2, 2) through the channel coupling effect.

III. ROTATIONAL AND VIBRATIONAL AUTOIONIZATIONS

In ZEKE spectroscopy, autoionization is considered as one of the main decay processes of the ZEKE states.[23] Figure 1(b) illustrates the transition from a ZEKE state of the higher IP to the ionization continuum of the lower IP. Our previous work[10] showed that this process can be induced by the breakdown of IBOA, which is defined by

$$\hat{H}'_{\text{IBO}}\Theta_{cw}\Phi_{cwm} \equiv -\frac{\hbar^2}{2m_e}\left(2\nabla_e\Theta_{cw}\cdot\nabla_e\Phi_{cwm} + \Phi_{cwm}\nabla^2_e\Theta_{cw}\right). \tag{3.1}$$

In this case, the equation of motion of $\hat{\rho}$ is given by Eq. (2.1), where $\hat{H} = \hat{H}_0 + \hat{H}'_{\text{IBO}}$.

In the autoionization of ZEKE states (represented by m or m'), the ZEKE states are coupled to the ionization continuum (represented by k). Thus from Eq. (2.1), we find

$$\frac{d\rho_{mm}}{dt} = -\frac{i}{\hbar}\sum_k (H'_{mk}\rho_{km} - H'_{km}\rho_{mk}) - \frac{i}{\hbar}\sum_{m'}\left(H'_{mm'}\rho_{m'm} - H'_{m'm}\rho_{mm'}\right) - \gamma_m\rho_{mm}, \tag{3.2}$$

where $\hat{H}'_{\text{IBO}}$ is denoted by $\hat{H}\prime$ and $\gamma_m = \Gamma^{mm}_{mm}$ represents the radiative rate constant. Similarly, we have

$$\frac{d\rho_{mk}}{dt} = -\left(i\omega_{mk} + \frac{1}{2}\gamma_m\right)\rho_{mk} + \frac{i}{\hbar}H'_{mk}\left(\rho_{mm} - \rho_{kk}\right) + \cdots \tag{3.3a}$$

and

$$\frac{d\rho_{mm'}}{dt} = -\left(i\omega_{mm'} + \gamma_{mm'}\right)\rho_{mm'}. \tag{3.3b}$$

By applying the Laplace transform, for example,

$$\bar{\rho}_{mm}(p) = \int_0^\infty e^{-pt}\rho_{mm}(t)dt, \tag{3.4}$$

we obtain

$$p\bar{\rho}_{mm} - \rho_{mm}(0) = -\frac{2}{\hbar}\text{Im}\sum_k H'_{km}\bar{\rho}_{mk} - \frac{2}{\hbar}\text{Im}\sum_{m'}H'_{m'm}\bar{\rho}_{mm'} - \gamma_m\bar{\rho}_{mm}, \tag{3.5}$$

$$p\bar{\rho}_{mk} - \rho_{mk}(0) = -\left(i\omega_{mk} + \frac{1}{2}\gamma_m\right)\bar{\rho}_{mk} + \frac{i}{\hbar}H'_{mk}\left(\bar{\rho}_{mm} - \bar{\rho}_{kk}\right), \tag{3.6a}$$

and

$$p\bar{\rho}_{mm'} - \rho_{mm'}(0) = -\left(i\omega_{mm'} + \gamma_{mm'}\right)\bar{\rho}_{mm'}, \tag{3.6b}$$

where $\gamma_{mm'} = (1/2)(\gamma_m + \gamma_{m\prime})$. The initial coherence can be created by optical excitation (or pumping) from a short-pulse laser (see Sec. V).

One can usually assume that $\rho_{mk}(0) = 0$; that is, no coherence is initially created. Eliminating $\bar{\rho}_{mk}(p)$ and $\bar{\rho}_{mm\prime}(p)$

from Eq. (3.5) yields

$$p\bar{\rho}_{mm} - \rho_{mm}(0) = \sum_k M_{mk}(p)(\bar{\rho}_{kk} - \bar{\rho}_{mm}) - \frac{2}{\hbar}\mathrm{Im}\sum_{m'}\left[\frac{H'_{m'm}\rho_{mm'}(0)}{p + i\omega_{mm'} + \gamma_{mm'}}\right] - \gamma_m\bar{\rho}_{mm}, \quad (3.7)$$

where $M_{mk}(p)$ denotes the memory kernel,

$$M_{mk}(p) = \mathrm{Im}\left[\frac{\frac{2i}{\hbar^2}|H'_{km}|^2}{p + i\omega_{mk} + \frac{\gamma_m}{2}}\right]. \quad (3.8)$$

It follows that

$$\frac{d\rho_{mm}}{dt} = \sum_k \int_0^t d\tau M_{mk}(\tau)[\rho_{kk}(t-\tau) - \rho_{mm}(t-\tau)] - \frac{2}{\hbar}\mathrm{Im}\sum_{m'} H'_{m'm}\rho_{mm'}(0)\exp[-t(i\omega_{mm'} + \gamma_{mm'})] - \gamma_m\rho_{mm}. \quad (3.9)$$

Since $\{k\}$ denotes the ionization continuum, the reversible process in Eq. (3.9) can be ignored,

$$\frac{d\rho_{mm}}{dt} = -\int_0^t d\tau M_{mm}(\tau)\rho_{mm}(t-\tau) - \gamma_m\rho_{mm}(t). \quad (3.10)$$

In the Markoff approximation,[25,33] Eq. (3.10) becomes *

$$\frac{d\rho_{mm}}{dt} = -W_m\rho_{mm}(t) - \gamma_m\rho_{mm}(t), \quad (3.11)$$

where

$$W_{mm} = \int_0^\infty dt \sum_k \mathrm{Im}\left[\frac{2i}{\hbar^2}|H'_{km}|^2 e^{-t(i\omega_{mk} + (1/2)\gamma_m)}\right] = \frac{2}{\hbar^2}\sum_k |H'_{km}|^2 D(\omega_{mk}), \quad (3.12)$$

$D(\omega_{mk})$ denotes the Lorentzian

$$D(\omega_{mk}) = \frac{1}{\pi}\frac{\gamma_m/2}{\omega_{mk}^2 + (\gamma_m/2)^2}, \quad (3.13)$$

and W_{mm} denotes the autoionization rate constant.

Equation (3.6b) indicates that, under proper conditions (e.g., using short excitation laser pulse), the quantum beat can be observed in the ZEKE spectroscopy, and this has indeed been observed experimentally.[34] It should be noted that the Schrödinger equation approach is not particularly suitable for treating coherence dynamics. In addition, based on the perturbation method, the Schrödinger equation approach can only provide rate constants (e.g., optical absorption rate constant, autoionization rate constant, and field ionization rate constant), and these rate constants have to be artificially inserted into the rate equations to obtain information on population or probability as a function of time. The coherence and damping effects are, however, not included. In the density matrix method, all the so-called rate equations are derived from the Liouville equation; in addition, the coherence effect and damping effect are automatically included. Furthermore, the density matrix method shows that the rate equations are valid only when the Markoff approximation is valid [see, for example, Eqs. (3.10) and (3.11)].

Next, we show how to evaluate the rotational and vibrational autoionizations. In Eq. (3.12), H'_{km} is given by

$$H'_{km} = \langle\Psi_{cw'k}|H'_{\mathrm{IBO}}|\Psi_{cwm}\rangle. \quad (3.14)$$

Here, the unperturbed bound wavefunction Ψ^0_{cwm} is defined by Eq. (2.12). Similarly, for the ionization continuum $\Psi^0_{cw'k}$, we have

$$|\Psi^0_{cwk}\rangle = |kl'\ v^{+\prime}N^{+\prime}J'M'_J\rangle = R_{kl'}(r)\chi_{v^{+\prime}}(R)\sum_{m'M^{+\prime}} C^{l'N^{+\prime}}_{m'M^{+\prime};J'\ M'_J} Y_{l'm'}(\theta,\phi) \times Y_{N^{+\prime}M^{+\prime}}(\Theta,\Phi). \quad (3.15)$$

In these expressions, $R_{kl'}$ represents the continuum electronic radial wavefunction, and other functions are defined similarly, as in Eq. (2.12). In Eqs. (2.12) and (3.15), the dependence of the electronic coordinate is completely removed from the ionic wavefunction (i.e., $\nabla_e\Theta^0_{cw} = 0$). Thus, to evaluate H'_{km}, we shall incorporate the first-order correction to the ionic wavefunciton by the multipole interaction V_p (for homonuclear diatomics, it is the quadrupole interaction V_{quad}). Then, Eq. (3.14) is shown as

$$\langle\Psi_{cw'k}|H'_{\mathrm{IBO}}|\Psi_{cwm}\rangle = -\frac{\hbar^2}{m_e}\frac{1}{E_{cw,cw'}}\left\langle\Phi^0_{cw'k}\middle|\left\langle\Theta^0_{cw'}\middle|\nabla_e V_p\middle|\Theta^0_{cw}\right\rangle\cdot\middle|\nabla_e\Phi^0_{cwm}\right\rangle, \quad (3.16)$$

where $E_{cw,cw'}$ represents the energy difference between the two ionic states and the second term in Eq (3.1) has vanished since $\nabla_e^2 V_p = 0$. For the rotational or vibrational autoionization of homonuclear diatomics, using the expressions in Eq. (3.15) the resulting matrix element can be expressed as

$$\langle kl'v^{+\prime}N^{+\prime}J\ M_J|\hat{H}'_{\mathrm{IBO}}|nl\ v^+N^+J\ M_J\rangle = -\frac{\hbar 2}{m_e}\frac{(-e)}{U^0_{v^+N^+} - U^0_{v^{+\prime}N^{+\prime}}}\langle\chi_{v^{+\prime}}|Q(R)|\chi_{v^+}\rangle \times\left[D_{l',l}\langle R_{kl'}|r^{-5}|R_{nl}\rangle - 3\left\langle R_{kl'}\middle|r^{-4}\middle|\frac{dR_{nl}}{dr}\right\rangle\right] \times g(l',N^{+\prime},J',M'_J;l,N^+,J,M_J), \quad (3.17)$$

where

$$D_{l,l} = 3\ ,\ D_{l+2,l} = -2l\ ,\ \text{and}\ D_{l-2,l} = 2(l+1). \quad (3.18)$$

Here, U^0_{v+N+} and $Q(R)$, respectively, denote the rovibrational energy and quadrupole moment of the ion core, and the definition of the factor g is the same as Eq. (2.14). The derivation of Eq. (3.17) is given in Ref. 10.

As an example, we consider the rotational and vibrational autoionizations of N_2. The physical quantities of N_2^+ were calculated by using the GAUSSIAN 03 package.[35] At

TABLE I. Rotational autoionization rate constant of N_2 for the transition of $\{nl, v^+ = 0, N^+ = 10, J = 10M_J\} \rightarrow \{kl, v^{+\prime} = 0, N^{\prime +} = 8, J = 10M_J\}$.

n	(cm^{-1})	ℓ	Rate (s^{-1})
100	60.79	2	1.653×10^8
100	60.79	3	2.221×10^7
100	60.79	4	4.736×10^6
100	60.79	5	1.342×10^6
100	60.79	6	4.569×10^5
100	60.79	7	1.764×10^5
100	60.79	8	7.424×10^4
100	60.79	9	3.316×10^4
100	60.79	10	1.539×10^4
200	68.92	2	2.066×10^7
200	68.92	3	2.777×10^6
200	68.92	4	5.921×10^5
200	68.92	5	1.677×10^5
200	68.92	6	5.714×10^4
200	68.92	7	2.206×10^4
200	68.92	8	9.288×10^3
200	68.92	9	4.150×10^3
200	68.92	10	1.928×10^3

the CCSD/aug-cc-pVDZ level, we obtained the equilibrium bond length $R_0 = 2.175$a.u., its quadrupole moment $Q(R_0) = 1.974$a.u., and $Q(R)$. Carrying out the numerical integrations of the electronic radial matrix elements, we obtained the numerical data for Eq. (3.17). The resulting autoionization rates are shown in Table I for rotational autoionization and Table II for vibrational autoionization. In both the tables, we only consider the dominant $l' = l$ transitions. For both rotational and vibrational autoionizations, we can see that the magnitude of the autoionization rate decreases significantly with increases in l. Since the high n bound radial wavefunctions are approximately proportional to $n^{-3/2}$, the rates of $n = 100$ are about eight times larger than those of $n = 200$ (the n^{-3} law). The propensity rule for the vibrational autoionization[36] indicates that the rate would decrease as $|\Delta v|$ increases. Therefore, the vibrational autoionization rates ($\Delta v = -1$) are about 2 orders of magnitude smaller than the rotational ones ($\Delta v = 0$).

TABLE II. Vibrational autoionization rate constant of N_2 for the transition of $\{nl, v^+ = 1, N^+ = 0, J = l\ M_J\} \rightarrow \{kl, v^{+\prime} = 0, N^{\prime +} = 2, J = l\ M_J\}$.

n	(cm^{-1})	ℓ	Rate (s^{-1})
100	2158	2	6.725×10^6
100	2158	3	7.458×10^5
100	2158	4	1.371×10^5
100	2158	5	3.161×10^4
100	2158	6	7.995×10^3
100	2158	7	2.056×10^3
100	2158	8	5.141×10^2
100	2158	9	1.215×10^2
100	2158	10	2.672×10^1
200	2166	2	8.407×10^5
200	2166	3	9.325×10^4
200	2166	4	1.714×10^4
200	2166	5	3.956×10^3
200	2166	6	1.002×10^3
200	2166	7	2.581×10^2
200	2166	8	6.471×10^1
200	2166	9	1.536×10^1
200	2166	10	3.394×10

From Eq. (2.14), we see that the autoionization rates depend also on the total rotational quantum number J. Other things unchanged, the rate constant is proportional to g^2. To demonstrate the dependence of J, we provide the radio of the g^2 factor for different J of a given l state. For example, for the case of $N^+ = 10$, $N\prime^+ = 8$, and $l = 2$, there are three possible values of J. The ratio of g^2 is, according to the formula, $g^2(J = 8)$: $g^2(J = 9)$: $g^2(J = 10) = 1 : 1.87 : 1.54$. Therefore, the g^2 factor is partly responsible for the J dependence.

In treating the autoionization of atoms and molecules, another approach based on the use of Fermi's golden rule and the electrostatic interaction (e.g., quadrupole and dipole interactions) is often used,[37] which, to the zero-order treatments, is equivalent to the above result. The equivalence of the two formulations and its physical implication are shown in Appendix A.

IV. *l*-LEVEL MIXING

In this section, we use the reduced density matrix method to study l-level mixing in the ZEKE spectroscopy. It is known that a stray electric field in ZEKE experiments could result in l-mixing and longer lifetimes of high Rydberg states.[38,39] In addition, an inhomogeneous field induced by ions could further lengthen the lifetime and cause the m-level mixing.[24,40] In this section, we focus on how to calculate l-mixing under the influence of a homogeneous field. We use the notations $L \equiv (lm)$ and $L' \equiv (l'm')$. Similar to the autoionization process, we start with

$$\frac{d\rho_{LL}}{dt} = -\frac{i}{\hbar}\sum_{L'}\left(H''_{LL'}\rho_{L'L} - H''_{L'L}\rho_{LL'}\right) - \sum_{L'}\Gamma_{LL}^{L'L'}\rho_{L'L'} \tag{4.1}$$

and

$$\frac{d\rho_{LL'}}{dt} = -\left(i\omega_{LL'} + \gamma_{LL'}\right)\rho_{LL'} + \frac{i}{\hbar}H''_{LL'}\left(\rho_{LL} - \rho_{L'L'}\right) + \cdots, \tag{4.2}$$

where $\hat{H}''$ denotes the Stark interaction between a stray field $\vec{E}_s$ and the ZEKE system,

$$\hat{H}'' = -\vec{\mu}\cdot\vec{E}_s. \tag{4.3}$$

In Eqs. (4.1) and (4.2), $-\Gamma_{LL}^{L'L'}$ denotes the decay rate constant for the transition $L' \rightarrow L$; in ZEKE spectroscopy, the decay rate includes both the autoionization and radiative processes and $\gamma_{LL'}$ represents the dephasing constant $\gamma_{LL'} = (1/2)(\Gamma_{LL}^{LL} + \Gamma_{L'L'}^{L'L'})$, where Γ_{LL}^{LL} and $\Gamma_{L'L'}^{L'L'}$ are the

total decay rate constants of L and $L\prime$, respectively. The pure dephasing has been ignored.

Notice that

$$\frac{d\rho_{LL'}}{dt} = -\left(i\omega_{LL'} + \gamma_{LL'}\right)\rho_{LL'} - \frac{i}{\hbar}\left(\vec{\mu}_{LL'}\cdot\ \vec{E}_s\right)\left(\rho_{LL} - \rho_{L'L'}\right) + \cdots. \quad (4.4)$$

Again, we use the Laplace transformation method to obtain

$$\frac{d\rho_{LL}}{dt} = \sum_{L'} W_{LL'}\left(\rho_{L'L'} - \rho_{LL}\right) - \sum_{L'}\Gamma_{LL}^{L'L'}\rho_{L'L'}, \quad (4.5)$$

where $W_{LL\prime}$ denotes the l-level mixing rate constant

$$W_{LL'} = \frac{2}{\hbar^2}|\vec{\mu}_{LL'}\cdot\ \vec{E}_s|^2\frac{\gamma_{LL'}}{\omega_{LL'}^2 + (\gamma_{LL'})^2}. \quad (4.6)$$

For convenience, Eq. (4.5) can be written as

$$\frac{d\rho_{lm,lm}}{dt} = \sum_{l'm'} W_{lm,l'm'}(\rho_{l'm',l'm'} - \rho_{lm,lm}) - \sum_{l'm'}\Gamma_{lm,lm}^{l'm',l'm'}\rho_{l'm',l'm'}, \quad (4.7)$$

where

$$W_{lm,l'm'} = \frac{2}{\hbar^2}|\vec{\mu}_{lm,l'm'}\cdot\ \vec{E}_s|^2\frac{\gamma_{lm,l'm'}}{\omega_{lm,l'm'}^2 + (\gamma_{lm,l'm'})^2}. \quad (4.8)$$

In most cases $\omega_{lm,l\prime m\prime} = 0$, unless the field is so strong that the electronic energy level is modified by $\vec{E}_s$. In addition, the transition dipole moment can be expressed as

$$-\vec{\mu}_{lm,l'm'}\cdot\ \vec{E}_s = eF\langle nl'm'|z|nlm\rangle, \quad (4.9)$$

where

$$\begin{aligned}&\langle nlm|\,z\,\left|nl'm'\right\rangle\\ &= -\frac{3}{2}n\sqrt{n^2-(l+1)^2}\sqrt{\frac{(l+1)^2-m^2}{(2l+1)(2l+3)}}a_0,\\ &\quad \text{if } l' = l+1, m' = m,\\ &= -\frac{3}{2}n\sqrt{n^2-l^2}\sqrt{\frac{l^2-m^2}{(2l-1)(2l+1)}}a_0,\\ &\quad \text{if } l' = l-1, m' = m,\end{aligned} \quad (4.10)$$

The selection rules in Eq. (4.10) allow coupling among l, while the mixing of m is forbidden.

Through Eqs. (4.1), (4.2) and (4.10), we can calculate the dynamic behavior of populations under the influence of a

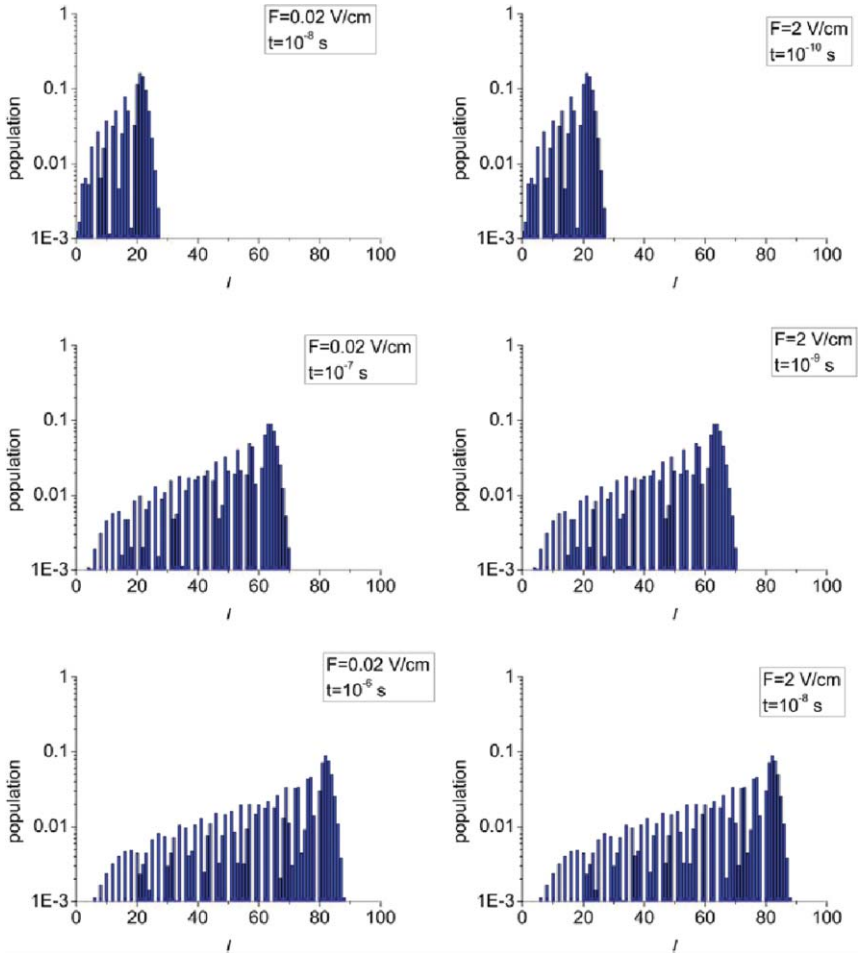

FIG. 2. Dynamic behavior of $n = 100$ population of H-atoms with a prepared state of $(l_0,m_0) = (0,0)$. The left panels show the population distributions along l at $F = 0.02$ V/cm and at various times. The right panels show the similar patterns at $F = 2$ V/cm.

stray field. These calculations require the decay rate constants Γ_{LL}^{LL} for the main dynamic processes. For example, for atoms, the radiative decay processes (e.g., spontaneous emission)[41] contribute, while, for molecular ZEKE states, the nonradiative decay processes (e.g., autoionization and predissociation)[23] dominate.

As an example, we first consider the l-mixing of H-atoms under a stray field. The main decay process for H-atoms is spontaneous emission, and related numerical data have been reported in Ref. 41. The dynamic behavior of l-mixing is exhibited in Fig. 2. First, we can see that as the time progresses (i.e., from the upper panels to the lower panels), the population propagates to higher l states. With a field value of $F = 0.02$ V/cm, the population propagates to the higher l states in 1 μs. With a larger field ($F = 2$ V/cm), the distribution time is about 0.01 μs. In addition, the patterns in the right panels are similar to those on the left; that is, the population distribution among the l states is determined by the product of time and the field strength. As the field strength increases, the corresponding time for the distribution is reduced.

Figure 3(a) shows the dynamic behaviors of total populations with different prepared states, indicating the typical exponential decay patterns. Due to the selection rule of m, the initial state (l_0, m_0) cannot mix with any state of $l < m_0$ (since $l = m_{\max} < m$). As a result, the total population with a lower m_0 would decay more rapidly, since it incorporates the short-lived, low-l states. For example, in the case of $(l_0, m_0) = (0, 0)$, the total decay rate is about 65 s^{-1}, while for $(l_0, m_0) = (10, 10)$ it is only about 0.1 s^{-1}.

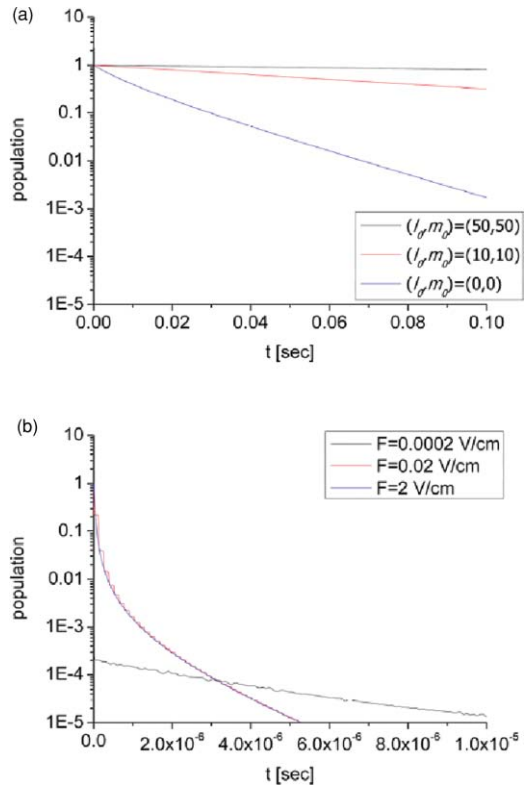

FIG. 3. (a) Dynamic behavior of the total population of H-atoms at $n = 100$, $F = 0.02$ V/cm with prepared states of $(l_0,m_0) = (50,50)$, $(10,10)$, $(0,0)$. (b) Dynamic behavior of the total population of H_2 at $n = 100$ with a prepared state $(l_0,m_0) = (1,0)$ at various F values.

Consider H_2 as an example for the l-mixing in molecular ZEKE states. The autoionization is the main decay process of H_2. The autoionization rate constants were numerically calculated for $l \leq 10$ and found to decrease rapidly as l increases. Using nonlinear modeling, for the state at $n = 100$, $N^+ = 2$, $m = M^+ = 0$, and $v^+ = 0$, we obtain the l scaling law for its rotational autoionization rate constant

$$\text{rate} = 2.204 \times 10^9 l^{-5.6}\ \text{s}^{-1}. \tag{4.11}$$

For $l = 1$, the rate is about 2×10^9 s^{-1}, but only 6×10^3 s^{-1} for $l = 10$. Therefore, in our calculations, the decay rate constant of $l > 10$ is negligible to the decay behavior of the total population.

Figure 3(b) presents the decay behavior of the total population with a prepared state $(l_0, m_0) = (1, 0)$ at various field F values. Here, we can see that the population decay curve of $F = 0.02$ V/cm overlaps that of $F = 2$ V/cm, which means that the influence of the electric field on the total decay rate is almost saturated at $F = 0.02$ V/cm. As in the case of $F = 0.0002$ V/cm, the Stark interaction is small. Therefore, a large portion of the population decays with the initial short-lived state $l = 1$. Only a small portion of the population would be distributed to the other l, which is shown as the long-tail of the curve of $F = 0.0002$ V/cm in Fig. 3(b).

In previous studies on l-mixing, the effective Hamiltonian method with experimentally determined quantum defects is commonly used to solve the time-dependent Schrödinger equation.[38,39] As pointed out by Chao *et al.*[11], this approach is equivalent to the Liouville equation, Eq. (2.1). However, in our formulation, we can see that the Liouville equation can be simplified by the Markoff approximation in the form of rate equations. Thus, with given decay rate constants, we can directly obtain the resulting population by solving Eq. (4.7). In addition, it should be noted that instead of the quantum defect, the decay rate constant of molecules can be calculated by the breakdown of IBOA.

V. OPTICAL ABSORPTION (OR PUMPING)

Figure 4 depicts three types of commonly used ZEKE spectroscopies. Type I represents the one-photon case, while types II and III represent the two-photon case. In type II, the first-step is resonant and in type III, the first-step is off-resonant. To treat the excitation (or pumping) process in the ZEKE spectroscopy, we again use the density matrix method. In this case, the density matrix of the observed system is determined by the equation of motion, Eq. (2.2), where $\hat{V}(t)$

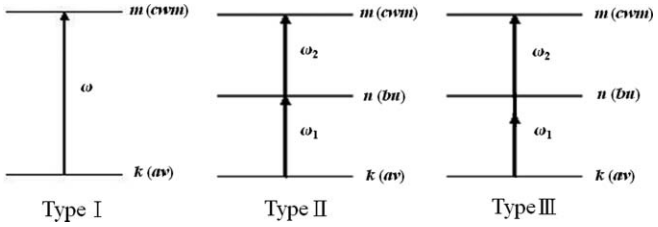

FIG. 4. ZEKE spectroscopies.

is the interaction between the molecule and the radiation field $\vec{E}(t)$.

We shall consider type I first. In the dipole approximation,

$$\hat{V}(t)' = -\vec{\mu}\cdot\ \vec{E}_0\cos\omega t = -\vec{\mu}\cdot\ [\vec{E}_0(\omega)e^{-it\omega} + \vec{E}_0(-\omega)e^{it\omega}], \tag{5.1}$$

where $\vec{\mu}$ is the dipole operator. Notice that

$$\frac{d\rho_{mm}}{dt} = -\frac{i}{\hbar}\sum_k (V_{mk}\rho_{km} - V_{km}\rho_{mk}) - \sum_l \Gamma^{ll}_{mm}\rho_{ll} \tag{5.2}$$

and

$$\frac{d\rho_{mk}}{dt} = -(i\omega_{mk} + \gamma_{mk})\rho_{mk} + \frac{i}{\hbar}V_{mk}(\rho_{mm} - \rho_{kk}) + \cdots, \tag{5.3}$$

where $\gamma_{mk} = \Gamma^{mk}_{mk}$ represents the dephasing constant, and

$$V_{mk} = -\vec{\mu}_{mk}\cdot\ \vec{E}_0\cos\omega t. \tag{5.4}$$

In the rotating wave approximation[25] and Markoff approximation, we obtain

$$\rho_{mk}(t) = -\frac{i}{4\hbar}\frac{\vec{\mu}_{mk}\cdot\ \vec{E}_0(\omega)e^{-it\omega}}{i(\omega_{mk}-\omega)+\gamma_{mk}}(\rho_{mm}-\rho_{kk}) + \cdots \tag{5.5}$$

and

$$\frac{d\rho_{mm}}{dt} = \sum_k W^{(1)}_{km}(\omega)(\rho_{kk} - \rho_{mm}) - \sum_l \Gamma^{ll}_{mm}\rho_{ll}, \tag{5.6}$$

where the absorption rate constant $W^{(1)}_{km}$ is given by

$$W^{(1)}_{km} = \frac{\pi}{2\hbar^2}|\vec{\mu}_{mk}\cdot\ \vec{E}_0|^2 D(\omega_{mk}-\omega), \tag{5.7}$$

and if a thermal equilibrium is involved, then

$$W^{(1)} = \sum_{\rm k}\sum_m P_k W^{(1)}_{km} = \frac{\pi}{2\hbar^2}\sum_{\rm k}\sum_m P_k|\vec{\mu}_{mk}\cdot\ \vec{E}_0|^2 D(\omega_{mk}-\omega), \tag{5.8}$$

where P_k denotes the Boltzmann distribution. The ρ_{mm} terms in the above master equation [i.e., Eq. (5.6)] describes the stimulated emission and can usually be omitted. Here, $D(\omega_{mk}-\omega)$ denotes the line-shape function (Lorentzian in this case),

$$D(\omega_{mk}-\omega) = \frac{1}{\pi}\frac{\gamma_{mk}}{\gamma^2_{mk} + (\omega_{mk}-\omega)^2}. \tag{5.9}$$

In the above equations, we can see that m is in IBOA, while k is in BOA. Γ^{ll}_{mm} describes the dynamics of the ZEKE states; in the collision-free condition, it involves the radiative transition and autoionization.

Section III mentions that the coherence can be created by optical pumping and its dynamics can exhibit a quantum beat behavior. Here, we show how this can be achieved. Notice that

$$\frac{d\rho_{mm'}}{dt} = -(i\omega_{mm'} + \gamma_{mm'})\rho_{mm'} - \frac{i}{\hbar}\sum_k (V_{mk}\rho_{km'} - V_{km'}\rho_{mk}). \tag{5.10}$$

Using Eq. (5.5), we obtain

$$\frac{d\rho_{mm'}}{dt} = -(i\omega_{mm'} + \gamma_{mm'})\rho_{mm'} + \frac{1}{4\hbar}\sum_k \left[\frac{(\vec{\mu}_{mk}\cdot\ \vec{E}_0(\omega))(\vec{\mu}_{km'}\cdot\ \vec{E}_0(-\omega))}{i(\omega_{km'}-\omega)+\gamma_{km'}}(\rho_{kk}-\rho_{m'm'}) - \frac{\left(\vec{\mu}_{mk}\cdot\ \vec{E}_0(\omega)\right)\left(\vec{\mu}_{km'}\cdot\ \vec{E}_0(-\omega)\right)}{i(\omega_{mk}-\omega)+\gamma_{mk}}(\rho_{mm}-\rho_{kk})\right], \tag{5.11}$$

which describes the dynamics of the coherence $\rho_{mm'}$, exhibiting the quantum beat due to the term $-(i\omega_{mm'} + \gamma_{mm'})\rho_{mm'}$.

Types II and can be treated similarly. For type II, using the second-order perturbation method, we obtain

$$\hat{V}(t) = -\vec{\mu}\cdot\ \vec{E}_{10}\cos\omega_1 t - \vec{\mu}\cdot\ \vec{E}_{20}\cos\omega_2 t, \tag{5.12}$$

$$W^{(2)}_{km} = \frac{\pi}{2\hbar^2}\left|\sum_n \frac{(\vec{\mu}_{mn}\cdot\vec{E}_{20})(\vec{\mu}_{nk}\cdot\vec{E}_{10})}{2\hbar(\omega_{nk} - i\gamma_{nk} - \omega_1)}\right|^2 \times D(\omega_{mk}-\omega_1-\omega_2), \tag{5.13}$$

$$W^{(2)} = \sum_{\rm k}\sum_m P_k W^{(2)}_{km}, \tag{5.14}$$

and similarly for type, we have

$$W^{(2)}_{km} = \frac{\pi}{2\hbar^2}\left|\sum_n \left[\frac{(\vec{\mu}_{mn}\cdot\vec{E}_{20})(\vec{\mu}_{nk}\cdot\vec{E}_{10})}{2\hbar(\omega_{nk}-\omega_1)} + \frac{(\vec{\mu}_{mn}\cdot\vec{E}_{10})(\vec{\mu}_{nk}\cdot\vec{E}_{20})}{2\hbar(\omega_{nk}-\omega_2)}\right]\right|^2 \times D(\omega_{mk}-\omega_1-\omega_2). \tag{5.15}$$

VI. IONIZATION OF ZEKE STATES BY DISCRIMINATION FIELD AND EXTRACTION FIELD

Sections III–V used the perturbation method to study optical absorption, l-level mixing, and autoionization. But this method cannot be used to treat the extraction field ionization of ZEKE states because, due to the high n values in this case, the field cannot be regarded as weak. The exact master equation for describing the extraction field ionization is presented as

$$\frac{d\hat{\rho}}{dt} = -\frac{i}{\hbar}[\hat{H}_0, \hat{\rho}] - \frac{i}{\hbar}[\hat{H}'', \hat{\rho}] - \hat{\Gamma}\hat{\rho} = -i\hat{L}\hat{\rho}, \tag{6.1}$$

where $\hat{H}''$ denotes the Stark Hamiltonian, while $\hat{H}_0$ and $\hat{\Gamma}$ were discussed in Secs. III–V. We introduce the projection operator $\hat{D}$ so that.

$$\hat{D}\hat{\rho} = \hat{\rho}_1(1-\hat{D})\hat{\rho} = \hat{\rho}_2, \tag{6.2}$$

where $\hat{\rho}_1$ denotes the collection of diagonal matrix elements of $\hat{\rho}$ (i.e., the population of the system), while $\hat{\rho}_2$ represents the collection of off-diagonal matrix elements of $\hat{\rho}$ (i.e., the coherence or phase of the system). It follows that Eq. (6.2) can be written as (Appendix B)

$$\hat{\rho}_1(t) = \exp[-t(i\hat{D}\hat{L} + \hat{W})]\hat{\rho}_1(0). \tag{6.3}$$

Here, the field ionization operator $\hat{W}$ is given by

$$\hat{W} = \int_0^\infty d\tau \hat{M}(\tau). \tag{6.4}$$

In other words, we can calculate the exact field-ionization rate constant from Eq. (6.4); it can also be evaluated perturbatively. Through the perturbation method, the master equations presented in the *l*-level mixing (discussed above) can be derived from Eq. (6.3).

Here, we calculate the field ionization rate constant through a frequently used semiclassical approach.[42,43] The electronic wave function $\Phi(\vec{r})$ satisfies the Schrödinger equation,

$$\left(-\frac{\hbar^2}{2m_e}\nabla_e^2 - \frac{Ze^2}{r} - eFz\right)\Phi(\vec{r}) = E\Phi(\vec{r}), \tag{6.5}$$

where $Z = 1$ is the charge and the electric field F lies along the z direction. The details of derivations are given in Appendix C. The field ionization rate constant is given by

$$W = |m|!\left(\frac{m_e e^2}{\hbar\sqrt{-2m_e E}}\right)^{|m|}|C|^2, \tag{6.6}$$

where the boundary condition and flux conservation give a value of C, which is given in Eq. (C.7).

Figure 5 shows the numerical results of the field ionization rate constant W in Eq. (6.6), with (C.7) for each corresponding field intensity region of [Fig. 5(a)] discrimination field ($0.1 < F < 3$ V/cm) and [Fig. 5(b)] extraction field ($2 < F < 10$ V/cm).[7,21] We first apply the discrimination field to remove electrons above the ionization potential threshold. We then observe the transmitted electrons by applying the extraction field, which is stronger than the discrimination field. We note that the principal quantum numbers corresponding to the ionization potential threshold for the discrimination and extraction fields are given by $F = (\hbar^2/16n^4 m_e e a_0^3)/10^2$. The electronic energy is given by $E = -(\hbar^2/2m_e a_0^2 n^2)$. The range of corresponding principal quantum numbers are $102 < n < 238$ for the discrimination field ($0.1 < F < 3$ V/cm) and $75 < n < 112$ for the extraction field ($2 < F < 10$ V/cm). In Fig. 5(a) we find that near the ionization potential threshold each curve increases rapidly and saturates at high intensity. From this, it seems reasonable to assume that most electrons above the ionization potential threshold have been removed. Here we remark that for more quantitative calculation of ionization rate constant we need to take Stark shift of potential energy curves and laser pulse shape into account. However, for our purpose here it is enough to specify a value of laser intensity at which most electrons above the ionization potential threshold are removed. According to our calculations, more than half (up to 80%) per unit time have been removed for cases $n = 120$, 150, and 200. Figure 5(b) shows a curve behavior similar to that in Fig. 5(a); that is, most electrons above the threshold can be transmitted and observed.

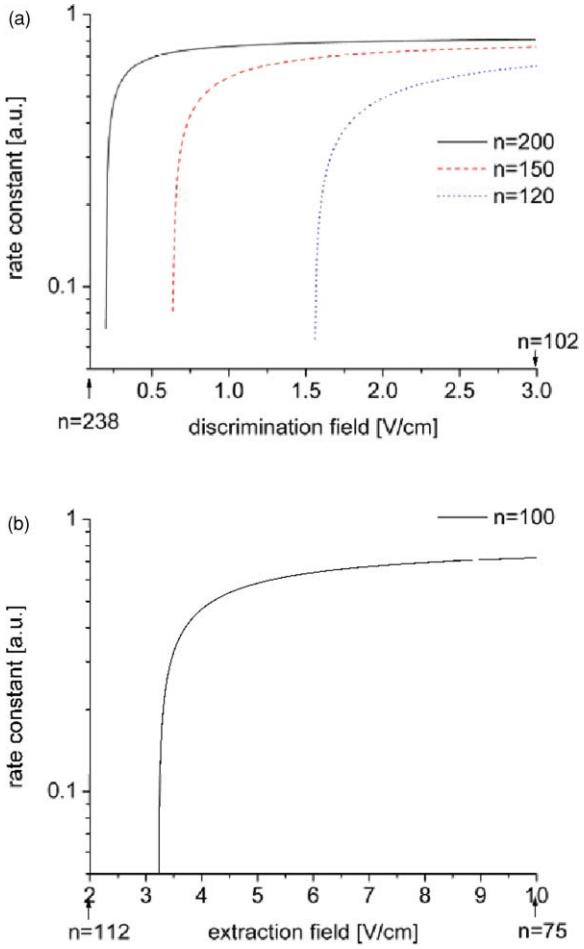

FIG. 5. (a) The calculated field ionization rate constants ($n = 120$, 150, 200) are plotted as a function of the discrimination field ($0.1 < F < 3$ V/cm). The electronic energy is given by $E = -(\hbar^2 a^2/2m_e n^2)$. (b) The calculated field ionization rate constant ($n = 100$) is plotted as a function of the extraction field ($2 < F < 10$ V/cm). The electronic energy is given by $E = -(\hbar^2 a^2/2m_e n^2)$. Here the atomic unit (a.u.) is used.

VII. CONCLUSION

Measurements of the ZEKE spectra involve optical absorption for the transition from the ground vibronic states to the ZEKE states, which may undergo autoionization and *l*-level mixing due to a stray field, and the ionization of the ZEKE states by a discrimination field and an extraction field, which yields the ZEKE electrons that determine the ZEKE spectra. Therefore, to simulate the ZEKE spectra, we should not only consider the absorption rate constant but also consider the dynamics of the ZEKE electrons. This paper presents the density matrix method to treat ZEKE spectroscopy and the dynamical processes involved. The density matrix method can provide information on the dynamics of the population

and coherence of the system, that is, the rate constants of all the processes involved in ZEKE spectroscopy. In other words, the density matrix method can describe the whole experiment under consideration and, by solving the equation of motion for the density matrix (conventionally called master equations), we can theoretically determine the ZEKE spectra. This paper presents the theoretical results of our preliminary attempts.

ACKNOWLEDGMENTS

The work of S.D.C and S.H.L was supported in part by the National Science Council of ROC and by the Deutsche Forschungsgemeinschaft (DFG). The work of Yi-Hsieh Wang and S. D. Chao is also partly supported by the CQSE National Taiwan University through 97R0066–66 and 99R80870.

APPENDIX A: PROOF OF EQUIVALENCE OF THE TWO FORMULATIONS MENTIONED IN SEC. III

Unlike in previous work, which used another formulation for the electron-core multiple interaction, we used the breakdown of IBOA (as described in Sec. III) to calculate the radiationless transition (autoionization) of the ZEKE states. Our previous paper showed that the two formulations are numerically and analytically equivalent.[10] Here, we use commutation relations to demonstrate this equivalence and its physical implications. From Eq. (3.17), we have

$$\langle \Psi_{cw'k}| \hat{H}'_{\mathrm{IBO}} |\Psi_{cwm}\rangle = -\frac{\hbar^2}{m_e}\frac{1}{E_{cw,cw'}}\left\langle \Theta^0_{c'w}\middle| \left\langle \Phi^0_k\middle| \nabla_e V_p \cdot \middle|\nabla_e \Phi^0_m\right\rangle \middle| \Theta^0_{cw}\right\rangle . \tag{A.1}$$

As reported by Russek *et al.*,[37] electrostatic interaction can be used as the perturbation in Fermi's golden rule. That is,

$$W_{(cwm\to cw'k)} = \frac{2\pi}{\hbar}\left|\langle \Psi_{cw'k}| \hat{V}'_p |\Psi_{cwm}\rangle\right|^2 \delta\left(E_{cw'k,cwm}\right). \tag{A.2}$$

From Ref. 10, we have

$$\left\langle \Phi^0_k\middle| V_p \middle|\hat{T}_e \Phi^0_m\right\rangle - \left\langle \hat{T}_e \Phi^0_k\middle| V_p \middle|\Phi^0_m\right\rangle = \left(E^0_m - E^0_k\right)\left\langle \Phi^0_k\middle| V_p \middle|\Phi^0_m\right\rangle \tag{A.3}$$

and

$$-\frac{\hbar^2}{2m_e}\left\langle \nabla^2_e \Phi^0_k\middle| V_p \middle|\Phi^0_m\right\rangle = -\frac{\hbar^2}{2m_e}\left[\left\langle \Phi^0_k\middle| V_p \middle|\nabla^2_e \Phi^0_m\right\rangle + 2\left\langle \Phi^0_k\middle| \nabla_e V_p \cdot \middle|\nabla \Phi^0_m\right\rangle + \left\langle \Phi^0_k\middle| \nabla^2_e V_p \middle|\Phi^0_m\right\rangle\right]. \tag{A.4}$$

Using the commutator expression for Eqs. (A.3) and (A.4), the resulting relations are given by

$$\left\langle \Phi^0_k\middle| \left[\hat{T}_e, \hat{V}_p\right] \middle|\Phi^0_m\right\rangle = \left\langle \Phi^0_k\middle| \left[\hat{H}^0_e, \hat{V}_p\right] \middle|\Phi^0_m\right\rangle = \left(E^0_k - E^0_m\right)\left\langle \Phi^0_k\middle| V_p \middle|\Phi^0_m\right\rangle, \tag{A.5}$$

$$\left\langle \Phi^0_k\middle| \left[\hat{T}_e, \hat{V}_p\right] \middle|\Phi^0_m\right\rangle = -\frac{\hbar^2}{2m_e}\left[2\left\langle \Phi^0_k\middle| \nabla_e V_p \cdot \middle|\nabla \Phi^0_m\right\rangle + \left\langle \Phi^0_k\middle| \nabla^2_e V_p \middle|\Phi^0_m\right\rangle\right]. \tag{A.6}$$

Incorporating the ionic wavefunctions to the matrix elements, we obtain

$$\left\langle \Psi^0_{cw'k}\middle| \left[\hat{T}_e, \hat{V}_p\right] \middle|\Psi^0_{cwm}\right\rangle = E_{cw,cw'}\left\langle \Psi^0_{cw'k}\middle| \hat{H}_{\mathrm{IBO}} \middle|\Psi^0_{cwm}\right\rangle = E_{km}\left\langle \Psi^0_{cw'k}\middle| V_p \middle|\Psi^0_{cwm}\right\rangle. \tag{A.7}$$

Since the energy difference between the ionic states is equal to that of the electronic states, as shown in Fig. 1(b), we can prove that

$$\left\langle \Psi^0_{cw'k}\middle| \hat{H}_{\mathrm{IBO}} \middle|\Psi^0_{cwm}\right\rangle = \left\langle \Psi^0_{cw'k}\middle| V_p \middle|\Psi^0_{cwm}\right\rangle. \tag{A.8}$$

Therefore, from Eq. (A.7), we conclude that the radiationless transition is attributed to the noncommutativity of the kinetic energy operator and the potential energy operator. Equation (A.2) presents it as the potential-energy representation, while Eq. (A.1) shows the kinetic-energy representation or the breakdown of IBOA.

APPENDIX B: DERIVATION OF EQ. (6.3)

Applying the Laplace transformation to Eq. (6.1) yields

$$p\hat{\rho}(p) - \hat{\rho}(0) = -i\hat{L}\hat{\rho}(p). \tag{B.1}$$

Referring to Eq. (6.2), Eq. (B.1) can be written as

$$p\bar{\rho}_1(p) - \hat{\rho}_1(0) = -i\hat{D}\hat{L}\bar{\rho}_1(p) - i\hat{D}\hat{L}\bar{\rho}_2(p) \tag{B.2}$$

and

$$p\bar{\rho}_2(p) - \hat{\rho}_2(0) = -i\left(1-\hat{D}\right)\hat{L}\bar{\rho}_1(p) - i\left(1-\hat{D}\right)\hat{L}\bar{\rho}_2(p). \tag{B.3}$$

Solving $\bar{\rho}_2(p)$ from Eq. (B.3), we obtain

$$\bar{\rho}_2(p) = \frac{1}{p + i\left(1-\hat{D}\right)\hat{L}}\rho_2(0) - \frac{1}{p + i\left(1-\hat{D}\right)\hat{L}} i\left(1-\hat{D}\right)\hat{L}\bar{\rho}_1(p). \tag{B.4}$$

Similarly, we assume that $\rho_2(0) = 0$ (that is, the random phase approximation). Substituting $\bar{\rho}_2(p)$ into Eq. (B.2) yields

$$p\bar{\rho}_1(p) - \rho_1(0) = -i\hat{D}\hat{L}\bar{\rho}_1(p) - \hat{M}(p)\bar{\rho}_1(p), \tag{B.5}$$

where $\hat{M}(p)$ denotes that memory kernel,

$$\hat{M}(p) = \hat{D}\hat{L}\frac{1}{p + i(1-\hat{D})\hat{L}}(1-\hat{D})\hat{L}. \tag{B.6}$$

It follows that

$$\frac{d\hat{\rho}_1}{dt} = -i\hat{D}\hat{L}\hat{\rho}_1 - \int_0^t d\tau \hat{M}(\tau)\hat{\rho}_1(t-\tau). \tag{B.7}$$

This is the exact master equation for the field-induced ionization of molecules and atoms. Alternatively, we have

$$\bar{\rho}_1(p) = \frac{1}{p + i\hat{D}\hat{L} + \hat{M}(p)}\hat{\rho}_1(0). \tag{B.8}$$

In the Markoff approximation, Eq. (B.7) becomes

$$\frac{d\hat{\rho}_1}{dt} = -i\hat{D}\hat{L}\hat{\rho}_1 - \hat{W}\hat{\rho}_1 \tag{B.9}$$

and

$$\bar{\rho}_1(p) = \frac{1}{p + i\hat{D}\hat{L} + \hat{W}}\hat{\rho}_1(0). \tag{B.10}$$

Carrying out the inverse Laplace transformation, we obtain

$$\hat{\rho}_1(t) = \exp[-t(i\hat{D}\hat{L} + \hat{W})]\hat{\rho}_1(0). \tag{B.11}$$

APPENDIX C: DERIVATION OF EQ. (6.6)

In parabolic coordinates Eq. (6.5) can be separated as,[42,43]

$$\xi = r + z,\ \eta = r - z,\ \Phi(\vec{r}) = \frac{\varphi(\xi)\chi(\eta)}{\sqrt{\xi\eta}}\frac{\exp(\pm im\phi)}{\sqrt{2\pi}}, \tag{C.1a}$$

$$\frac{\hbar^2}{m_e}\frac{\partial^2}{\partial\xi^2}\varphi + \left(\frac{E}{2} + \frac{\beta_1}{\xi} + \frac{\hbar^2}{4m_e\xi^2} + \frac{eF}{4}\xi\right)\varphi = 0, \tag{C.1b}$$

$$\frac{\hbar^2}{m_e}\frac{\partial^2}{\partial\eta^2}\chi + \left(\frac{E}{2} + \frac{\beta_2}{\eta} + \frac{\hbar^2}{4m_e\eta^2} - \frac{eF}{4}\eta\right)\chi = 0, \tag{C.1c}$$

where ϕ is the angular coordinate, m is the projection quantum number to the z-axis, and $\beta_1 + \beta_2 = Ze^2$. The asymptotic form of the wave function $\Phi(\vec{r})$ for $z \gg 1$ (Ref. 42) is given by

$$\Phi(\vec{r})\xi^{\frac{Ze^2m_e}{\hbar\sqrt{-2m_eE}}-1-|m|/2}\exp\left(-\frac{\sqrt{-2m_eE}}{2\hbar}\xi\right)\eta^{|m|/2} \times\exp\left(-\frac{\sqrt{-2m_eE}}{2\hbar}\eta\right)\frac{\exp(\pm im\phi)}{\sqrt{2\pi}}, \tag{C.2}$$

where $\xi \gg \eta$. From Eqs. (C.1) and (C.2), we obtain

$$\beta_1 = Ze^2 - \frac{\hbar}{2m_e}\sqrt{-2m_eE}(|m|+1),\ \beta_2 = \frac{\hbar}{2m_e}\sqrt{-2m_eE}(|m|+1). \tag{C.3}$$

Near the z axis, the surface integral is $dS = \rho d\rho d\phi = (1/2)\xi d\eta d\phi$, since $\eta\tilde{\rho}^2/\xi$, where ρ is the distance from z axis. The function χ behaves like $\chi = \eta^{(|m|+1)/2}\exp\left(-(\sqrt{-2m_eE}/2\hbar)\eta\right)$, and the probability of transition per unit time is given by

$$W = \frac{i\hbar}{2m_e}\left(\varphi\frac{d\varphi^*}{d\xi} - \varphi^*\frac{d\varphi}{d\xi}\right)|m|!\left(\frac{m_ee^2}{\hbar\sqrt{-2m_eE}}\right)^{|m|}. \tag{C.4}$$

The semiclassical solution for φ, i.e., $\varphi = (C\sqrt{m_e}/\sqrt{p(\xi)})\exp(\frac{i}{\hbar}\int^\xi d\xi' p(\xi'))$ with $p(\xi) = \sqrt{(m_eE/2) + (\beta_1/\xi) + (eF/4)\xi}$ provides the field ionization rate constant in Eq. (6.6)

For over potential barrier scattering, $|C|^2$ is calculated as the transmission probability for large z. Thus φ is written as

$$\varphi(\xi) = \frac{\sqrt{m_e}}{\sqrt{p(\xi)}}\left(\exp\left(\frac{i}{\hbar}\int_{\xi_F}^{\xi} p(\xi')d\xi'\right) + r\exp\left(-\frac{i}{\hbar}\int_{\xi_F}^{\xi} p(\xi')d\xi'\right)\right)\ (\xi < \xi_F),$$

$$\varphi(\xi) = C\frac{\sqrt{m_e}}{\sqrt{p_F}}\exp\left(\frac{i}{\hbar}\int_{\xi_F}^{\xi} p_F d\xi'\right)\ (\xi > \xi_F), \tag{C.5}$$

where r is the coefficient of a reflected wave. We assume that for $\xi > \xi_F$, the wave function is asymptotically free and connected at $\xi = \xi_F$. $p(\xi)$ has a maximum at $\xi = \xi_c$, and $\xi_c \ll \xi_F$. Then p_F is defined as $p_F \equiv p(\xi_c)$. The boundary condition and flux conservation at $\xi = \xi_F$ give

$$1 - |r|^2 = |C|^2, \tag{C.6a}$$

$$r = \frac{i\left(\sqrt{\frac{p(\xi_F)}{p_F}} - \sqrt{\frac{p_F}{p(\xi_F)}}\right) - \frac{p(\xi_F)'}{2p(\xi_F)^2}\sqrt{\frac{p(\xi_F)}{p_F}}}{i\left(\sqrt{\frac{p(\xi_F)}{p_F}} + \sqrt{\frac{p_F}{p(\xi_F)}}\right) + \frac{p(\xi_F)'}{2p(\xi_F)^2}\sqrt{\frac{p(\xi_F)}{p_F}}}, \tag{C.6b}$$

$$C = \frac{2i}{i\left(\sqrt{\frac{p(\xi_F)}{p_F}} + \sqrt{\frac{p_F}{p(\xi_F)}}\right) + \frac{p(\xi_F)'}{2p(\xi_F)^2}\sqrt{\frac{p(\xi_F)}{p_F}}}. \tag{C.6c}$$

[1] K. Müller-Dethlefs, M. Sander, and E. W. Schlag, Chem. Phys. Lett. **112**, 291 (1984).
[2] E. W. Schlag, *ZEKE Spectroscopy* (Cambridge University Press, Cambridge, 1998).
[3] S. Willitsch, A. Wuest, and F. Merkt, Chimia **58**, 281 (2004).
[4] R. C. Shiell, X. K. Hu, Q. C. J Hu, and J. W. Hepburn, Faraday Discuss. **115**, 331 (2000).
[5] L. Schneider, W. Meier, E. Wrede, K. H. Welge, M. N. R. Ashfold, and C. M. Western, J. Chem. Phys. **92**, 7027 (1990).
[6] S. A. Harich, D. X. Dai, C. C. Wang, X. Yang, S. D. Chao, and R. T. Skodje, Nature (London) **419**, 281 (2002).
[7] F. Merkt and T. P. Softley, Int. Rev. Phys. Chem. **12**, 205 (1993).
[8] S. T. Pratt, Annu. Rev. Phys. Chem. **56**, 281 (2005).
[9] S. D. Chao, H. L. Selzle, H. J. Neusser, E. W. Schlag, L. Yao, and S. H. Lin, Z. Phys. Chem. **221**, 633 (2007).
[10] Yi-Hsieh Wang, Y. Teranishi, H. Mineo, S. D. Chao, H. L. Selzle, H. J. Neusser, E. W. Schlag, and S. H. Lin, Chem. Phys. Lett. **486**, 104 (2010).

[11]S. D. Chao, M. Hayashi, S. H. Lin, and E. W. Schlag, J. Chin. Chem. Soc. (Taipei) **45**, 491 (1998).
[12]F. Remacle and R. D. Levine, Int. J. Quantum Chem. **67**, 85 (1998).
[13]S. Fredin, D. Gauyacq, M. Horani, Ch. Jungen, G. Lefevre, and F. Masnou-Seeuws, Mol. Phys. **60**, 825 (1987).
[14]A. Kirrander, H. H. Fielding, and Ch. Jungen, J. Chem. Phys. **127**, 164301 (2007).
[15]J. Xie and R. N. Zare, J. Chem. Phys. **93**, 3033 (1990).
[16]J. Xie and R. N. Zare, J. Chem. Phys. **97**, 2891 (1992).
[17]A. D. Buckingham, B. J. Orr, and J. M. Sichel, Philos. Trans. R. Soc. London, Ser. A **268**, 147 (1970).
[18]J. M. Sichel, Mol. Phys. **18**, 95 (1970).
[19]M. S. Ford and K. Müller-Dethlefs, Phys. Chem. Chem. Phys. **6**, 23 (2004).
[20]M. S. Ford, R. Lindner, and K. Müller-Dethlefs, Mol. Phys. **101**, 705 (2003).
[21]F. Merkt and T. P. Softley, J. Chem. Phys. **96**, 4149 (1992).
[22]F. Merkt and T. P. Softley, Phys. Rev. A **46**, 302 (1992).
[23]T. P. Softley, Int. Rev. Phys. Chem. **23**, 1 (2004).
[24]W. A. Chupka, J. Chem. Phys. **98**, 4520 (1993).
[25]S. H. Lin, R. Alden, R. Islampour, H. Ma, and A. A. Villaeys, *Density Matrix Method and Femtosecond Processes* (World Scientific, Singapore, 1991).
[26]S. H. Lin, C. H. Chang, K. K. Liang, R. Chang, Y. J. Shiu, J. M. Zhang, T. S. Yang, M. Hayashi, and F. C. Hsu, Adv. Chem. Phys. **121**, 1 (2002).
[27]M. Bixon and J. Jortner, Mol. Phys **89**, 373 (1996).
[28]S. H. Lin, J. Chem. Phys. **44**, 3759 (1966).
[29]T. P. Softley and A. J. Hudson, J. Chem. Phys. **101**, 923 (1994).
[30]C. R. Mahon, G. R. Janik, and T. F. Gallagher, Phys. Rev. A **41**, 3746 (1990).
[31]D. R. Bates and G. Poots, Proc. Phys. Soc., London, Sect. A **66**, 784 (1953).
[32]E. E. Eyler and F. M. Pipkin, Phys. Rev. A **27**, 2462 (1983).
[33]A. Boeglin, B. Fain, and S. H. Lin, J. Chem. Phys. **84**, 4838 (1986).
[34]M. J. J. Vrakking, D. M. Villeneuve, and A. Stolow, Phys. Rev. A **54**, R37 (1996).
[35]M. J. Frisch, G. W. Trucks, H. B. Schlegel, *et al.*, GAUSSIAN 03, Revision C.2, Gaussian, Inc., Pittsburgh, PA, 2003.
[36]R. S. Berry, J. Chem. Phys. **45**, 1228 (1966).
[37]A. Russek, M. R. Patterson, and R. L. Becker, Phys. Rev. **167**, 17 (1968).
[38]M. Bixon and J. Jortner, J. Chem. Phys. **105**, 1363 (1996).
[39]M. J. J. Vrakking, J. Chem. Phys. **105**, 7336 (1996).
[40]F. Merkt and R. N. Zare, J. Chem. Phys. **101**, 3495 (1994).
[41]S. D. Chao, S. H. Lin, H. L. Selzle, and E. W. Schlag, Chem. Phys. Lett. **265**, 445 (1997).
[42]B. M. Smirnov and M. I. Chibisov, Sov. Phys. JETP **22**, 585 (1966).
[43]H. A. Bethe and E. E. Salpeter, *Quantum Mechanics of One- and Two-Electron Atom* (Dover, New York, 2008).